Sensitive harmonic detection of ammonia trace using a compact photoacoustic resonator at double-pass configuration and a wavelength-modulated distributed feedback diode laser

G. R. Lima · L. Mota · A. Miklós · J. Angster ·
Z. Dubovski · M. G. da Silva · M. Sthel ·
H. Vargas

Abstract A sensitive detection of ammonia in parts per billion by volume is described. The system based on photoacoustic spectroscopy (PAS) consists of distributed feedback laser diode emitting near 1,531.7 nm and a compact PA cell at double-pass configuration. In order to optimize the signal background ratio of the system, two types of modulations were tested, amplitude and wavelength modulations (WM). Using a digital lock-in amplifier, the $1f$ and $2f$ detection in WM could be investigated. A detection limit of 470 parts per million by volume could be achieved at WM-$2f$. In the sense of quantifing the adsorption–desorption process, the response time of the system and detection accuracy was performed in different flows. Response times between 10 and 49 s, depending on the flow rate, were obtained which enables the PA system to measure low concentrations of ammonia with high accuracy in real time.

1 Introduction

The real-time monitoring of ammonia (NH_3) emissions has found many industrial, environmental and medical

G. R. Lima (✉) · L. Mota · M. G. da Silva · M. Sthel ·
H. Vargas
Laboratório de Ciências Físicas, Universidade Estadual do Norte
Fluminense Darcy Ribeiro, Av. Alberto Lamego, 2000, Parque
Califórnia, Campos dos Goytacazes, Rio de Janeiro 28013-602,
Brazil
e-mail: guiuenf@yahoo.com.br

A. Miklós · J. Angster · Z. Dubovski
Fraunhofer Institut für Bauphysik, Universität Stuttgart,
Nobelstraβe, 12, Vaihingen, 70569 Stuttgart,
Baden Württemberg, Germany

applications. In the semiconductor industry, even low amounts of NH_3 are enough to reduce the performance of lithographic process [1], while in the environment, it might affect the soil acidity [2]. In medicine, for instance, the NH_3 concentration on the human breath is associated with renal conditions and its real-time monitoring may be useful for a medical diagnostic to determine the efficacy and endpoint of hemodialysis treatment [3]. Therefore, techniques for detecting gases at trace levels are needed.

Currently, different methods have been applied for trace gas sensing, being the photoacoustic spectroscopy (PAS) a worldwide established one. This is because PAS offers several advantages such as increased sensitivity and selectivity, stability, fast response, wide dynamic range, beyond it allows real-time measurements. Besides, the development of laser technology provides new tunable radiation sources that improve the PAS system. For example, the distributed feedback (DFB) semiconductor diode laser has a compact size, low weight, high spectral resolution and no cooling requirements [4–6]. These features are extremely important to buildup a robust and compact PA spectrometer for detecting trace gases in situ.

Another point to be concerned is the detection of low ammonia concentration, which still represents a technical-scientific challenge. Due to the polar nature of this gas, adsorption–desorption effect can be a limiting factor in the gas detection. Some precautions must be taken to minimize this effect, primarily by choosing materials that avoid the adsorption of polar molecules for the inner surface of the PA cell, tubes and connections, by heating the PA resonator and by operating in continuous flow mode at high flow rates [7, 8]. Also, new PA sensor constructions have been developed to minimize adsorption–desorption effects, using, for example, high quality Teflon in the inner surface

and tangential sample injection into the cylindrical resonator of the PA cell [9].

So, this work focuses on the combination of a compact differential PA cell at double-pass configuration with a DFB laser operating in both amplitude (AM) and wavelength (WM) modes for detecting NH_3 at atmospheric pressure. In WM, first (1f) and second (2f) harmonic detections are employed by means of a lock-in amplifier. Additionally, in order to quantify the adsorption–desorption effect, the response time of the PA cell at different conditions is also investigated.

2 Photoacoustic spectroscopy: PAS

PAS is an absorption technique based on PA effect. The theoretical concept of this technique has been described by many authors [10–15]. In brief, the PA signal is generated when a modulated light beam goes through the PA cell. The interaction between radiation and matter, in this case gases, results in a molecular absorption of the light and excitation of the absorbing molecules to a higher energy level. The nonradiative relaxation process of the excited states is dominant, and the energy previously absorbed is converted into heat in the sample. Therefore, a periodic heating of the sample is produced, which leads to a pressure variation [15, 16].

The pressure oscillation inside the PA cell can be detected by microphones and monitored by a lock-in amplifier. Then, PA signal S can be described as

$$S(\lambda) = S_m P_l C_{cell} N_{tot} c \sigma(\lambda) \tag{1}$$

where, S_m is the microphone sensitivity, P_l is the laser power, C_{cell} is the PA cell response constant, N_{tot} is the total density of molecules, c and $\sigma(\lambda)$ are the concentration and absorption cross section of the investigated gas, respectively [17]. The cross section depends on the wavelength λ of the radiation.

Wavelength modulation technique using harmonic detection is one of the most effective methods to minimize the background signal. Some lasers, such as DFB diodes, offer the possibility to be wavelength modulated by feeding their injection current with a reduced modulation amplitude. The most applied waveform for this kind of modulation is the sinusoidal form. With the aim of improving the sensitivity of the PA system, other modulation waveforms for this application have been reported in the literature, i.e., square, modified square, triangle waves and composition of functions [18]. However, the best modulation waveform depends on the line shape of the molecular absorption.

In the case of the sinusoidal waveform, the wavelength of the laser can be written as:

$$\lambda(t) = \lambda_c + \lambda_0 \cos(2\pi f t) \tag{2}$$

where $\lambda(t)$ stands for the instantaneous wavelength of the laser, λ_c is the central wavelength, λ_0 is the modulation amplitude, and f is the sinusoidal modulation frequency.

The WM theory is well documented in the literature [19, 20]. The first theoretical models were presented by Arndt [21] and Reid and Labrie [23], using an approach for exclusive WM. Thereafter, more complete theoretical models taking into account for the contribution of AM in WM were presented by Philippe and Hanson [24] based on Fourier decomposition.

3 Experimental details

A distributed feedback (DFB) InGaAsP/InP diode laser (EM4 high power DFB, E0038143, AA1401, temperature ranges from 20 to 40 C, the maximum power is about 80 mW at 1,533.7 nm) is used as radiation source. The laser chip, a monitor photodiode and a Peltier element are placed onto a metal housing equipped with butterfly connections. The laser light is coupled through an optical fiber (PM 250, core diameter 8 μm), and it is mounted on a butterfly-like mounting (Thorlabs, LM 1452). The modulation and temperature control of the laser can be managed by a diode laser driver (Melles Griot, 06 DLD 103). The DFB laser is fiber coupled and adapted to a collimator that could be directly positioned in the PA cell, easing the alignment of the system.

The compact size differential PA cell (6.6 cm × 5.4 cm × 3.0 cm) is shown in Fig. 1. With a resonance quality factor (Q) of about 10, the PA cell was used in a resonant configuration exciting its first longitudinal acoustic mode at 6.49 kHz. Basically, the PA cell is composed of two calcium fluoride (CaF_2) optical windows, gas inlet and outlet and two resonators. The resonators have cylindrical shape with 23.2 mm length and 3.8 mm diameter and are equipped with microphones (Knowles Electronics, TM 24547-C36) located in the middle of the resonators. The microphones were carefully selected, in order to have the same frequency response. The laser passes through a single resonator generating the photoacoustic signal plus background of the system. In the second resonator, only the background is measured. By the difference of both microphone signals, the contribution of the background can be significantly reduced, increasing the signal-to-standard deviation of the background ratio ($SSD_{Bg}R$).

With the aim of minimizing turbulence noise caused by gas flow into the cell, this PA cell has four acoustic buffers and two $\lambda/4$ acoustic filters. Moreover, the inner surface of the cell is covered by a PTFE (Polytetrafluoroethylene, Teflon) coating. Another characteristic of this PA cell is the

Fig. 1 Scheme of differential PA cell at double-pass configuration
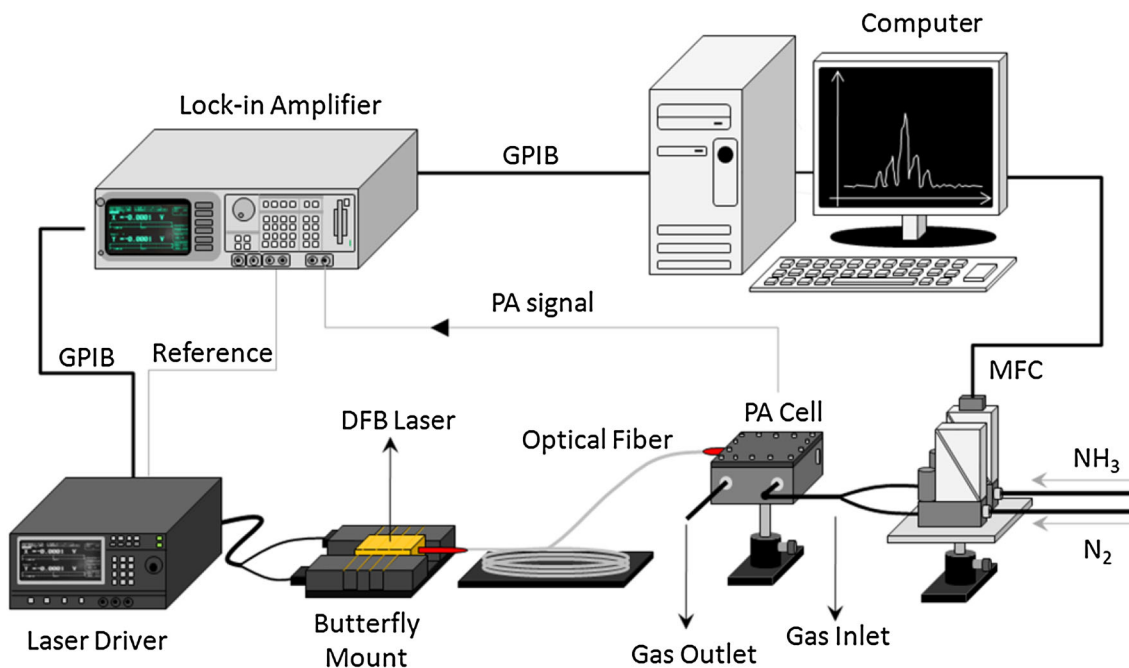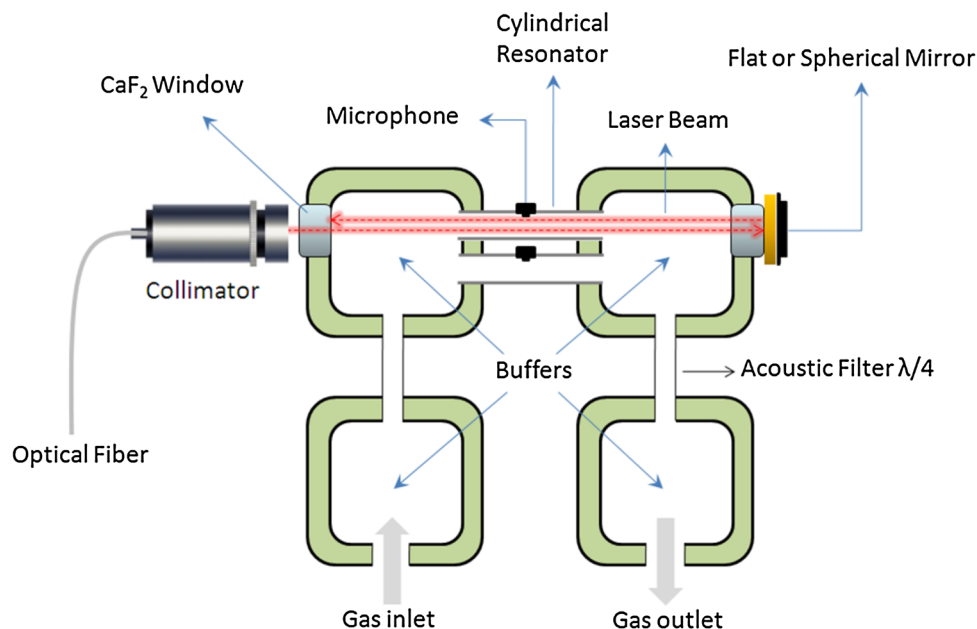
Fig. 2 Experimental setup

possibility to use double-pass configuration by inserting a reflecting mirror behind the output CaF_2 window. Two mirrors were tested as a way of improving the detection sensitivity, i.e., a flat gold coated and a concave spherical aluminum coated with 40-mm focal length.

A digital lock-in amplifier (Stanford Research Systems, SR850) at differential input mode was used to measure the signal using phase-sensitive detection with an integration time of 300 ms for all measurements. It was connected to a

computer and the laser driver by general purpose interface bus (GPIB) connection. The experimental data points were collected by a homemade software written under Lab-VIEW 8.6 platform.

WM was performed by modulating the injection current of the laser by a sinusoidal waveform of the built-in oscillator of the lock-in, while AM was achieved by switching the laser current on and off, by means of the digital modulation function of the laser driver.

The gas handling system consisted of two gas cylinders filled with certified mixtures of 50 and 1,000 parts per million by volume (ppmv) of NH_3 buffered in nitrogen (N_2) purchased from the Linde Group, Germany. NH_3 concentrations down to sub-ppmv range could be achieved by diluting the certified ammonia mixture with pure N_2 through the computer controllable mass flow controllers (MFC, EL-Flow Bronkhorst, F201CV-200 and F201CV-050) with maximal flow rate of 200 and 50 standard cubic centimeter (sccm). The experimental setup used in this work is shown in Fig. 2.

4 Results and discussion

First, AM was conducted. To do so, the laser was digitally square wave modulated by the laser driver between 50 and 350 mA, being the lower value the laser emission threshold current. Ammonia (1,000 ppmv) spectrum was recorded by scanning the laser temperature between 20 and 35 °C using the built-in Peltier element of the DFB laser. The temperature range could be assigned to the wavelength between 1,531.2 and 1,532.7 nm.

Figure 3a shows the absorbance spectrum for NH_3 1 ppmv taken from the Northwest-infrared database [27], and Fig. 3b presents the photoacoustic spectrum as a function of wavelength. Both spectra were normalized to their respective maximum values. Two ammonia absorption features can be identified in the PA spectrum. The comparison with the Northwest database spectrum allowed the conversion of the diode laser from temperature to wavelength. However, a pressure broadening of the absorption features of the PA spectrum can be observed.

In order to improve the sensor performance, the modulation amplitude was optimized to maximize $SSD_{Bg}R$. For the evaluations, measurements in AM and WM combined with first (1f) and second (2f) harmonic detections were undertaken. By means of a digital lock-in amplifier (Stanford SR850), a sinusoidal waveform at different modulation amplitudes, i.e., 1.67, 3.33, 4.97, 6.59, 8.20 and 9.79 mA was employed to feed the laser. As the laser wavelength is dependent upon the laser current, these current amplitudes promote different values of amplitude modulation on the wavelength. Moreover, a double-pass configuration was used; this is achieved through the insertion of a reflecting mirror behind the output CaF_2 window that the cell comprises. In this sense, two mirrors were tested, i.e., a gold-coated flat and an aluminum-coated spherical with 40 mm of focal length. All measurements were taken using 1,000 ppmv ammonia at 200 sccm flow rate. The results are summarized in Fig. 4.

The best $SSD_{Bg}R$ was achieved using WM-2f with 8.20 mA of modulation amplitude, associated with
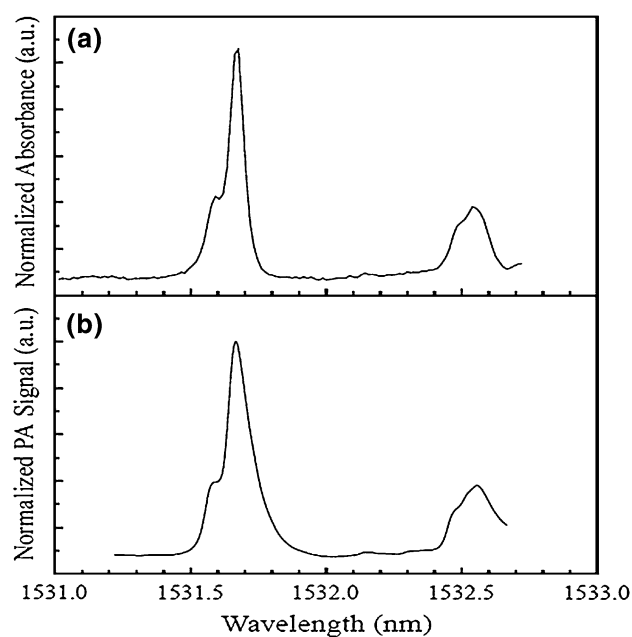
Fig. 3 **a** Normalized absorbance spectrum from Pacific Northwest National database for 1 ppmv at 25 °C and **b** normalized PA spectrum for 1,000 ppmv of ammonia using a spherical mirror

spherical mirror. It was observed during these measurements that the PA signal is higher in WM-1f when compared with WM-2f.

In WM, the laser frequency is modulated with f and the background occurs at the same frequency. However, the PA signals are demodulated at the frequency 2f. Thus, by demodulating the microphone signal at 2f, the acoustic response from the window and walls of the PA cell absorption can be avoided [22]. Background signals in WM-1f and WM-2f at different modulation amplitudes are shown in Fig. 5. While the background is constant in WM-2f, it increases linearly with the modulation amplitude in WM-1f.

As predicted by the theory [23], the PA spectra measured at small modulation amplitudes in WM-1f and WM-2f are proportional to the first and second derivative, respectively, of the absorption feature seen in AM (see Fig. 6).

The detection limit may be significantly enhanced by reducing the background (Bg) down to the level of the electronic noise. This is accomplished when WM is used. However, the power of the diode laser is current dependent. Thus, not only the wavelength but also the laser power is modulated due to the modulation of the injection current of the laser. This produces a residual AM [24], which is responsible for the Bg signal clearly observed in Fig. 7. The AM contribution to the photoacoustic signal increases as the modulation amplitude becomes larger. Then, the broadening becomes dominant and the PA signal spectrum

Fig. 4 Results of SSD$_{Bg}$R for different modulations depths. The *x*-axis is not applicable to AM; however, two lines were plotted to represent the value of SSD$_{Bg}$R for AM.
(*S* photoacoustic signal, *Bg* background, SD_{Bg} is the standard deviation of the background)
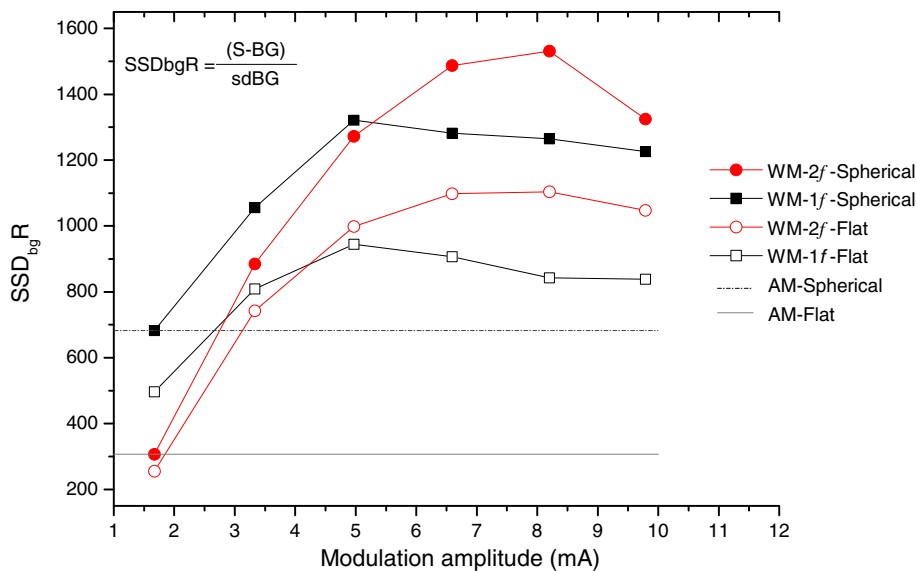
Fig. 5 Background signals in WM-1*f* and WM-2*f* at different modulation amplitudes. These measurements were taken using pure N$_2$ at 100 sccm flow rate
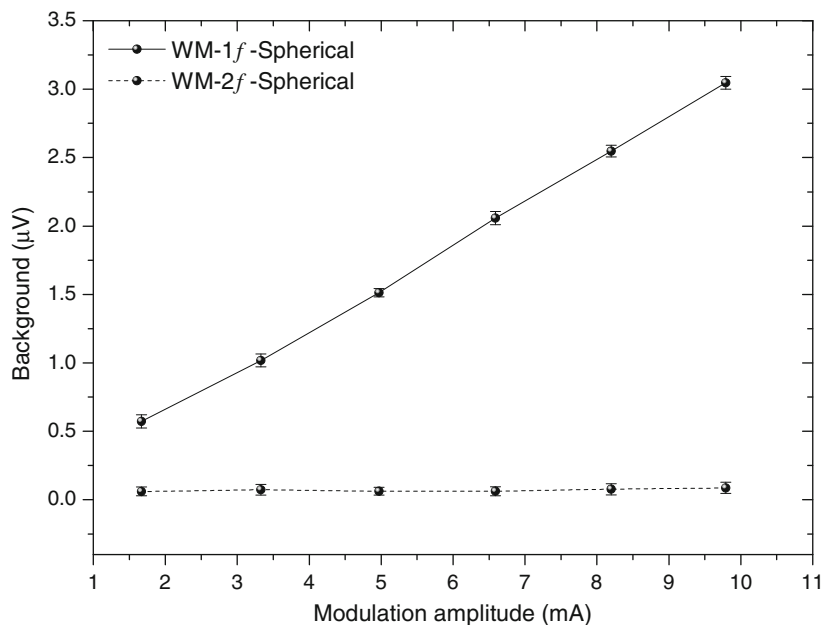

looses the derivative profile, and the absorption features become very similar to the PA spectrum observed using only AM [25]. Therefore, the modulation amplitude can be optimized to the sensitivity and selectivity requirements depending upon the application.

The ammonia detection limit was obtained in the optimized configuration, i.e., WM-2*f* and 8.2 mA of modulation amplitude. In this measurement, a certified mixture of ammonia buffered in N$_2$ was diluted in pure N$_2$ using mass flow controllers. Eighteen concentration steps starting from 12 to 124 ppbv were obtained with 100 sccm total flux. The temperature of the laser was kept constant at

21.98 ± 0.02 °C in order to stabilize the wavelength at the ammonia absorption peak.

The temperature dependence of the laser wavelength was 0.1 nm/°C, and the corresponding wavelength fluctuation was ±0.002 nm. As this value is very small compared with the full width at half maximum (FWHM) of the main absorption peak (∼0.130 nm), the PA signal oscillation caused by wavelength fluctuations was small.

Since the background related to windows and cell walls absorptions is typically coherent with the laser radiation, it has a stable phase lag of θ_B to the lock-in reference and the PA signal has another constant phase θ_{PA}, Therefore, the
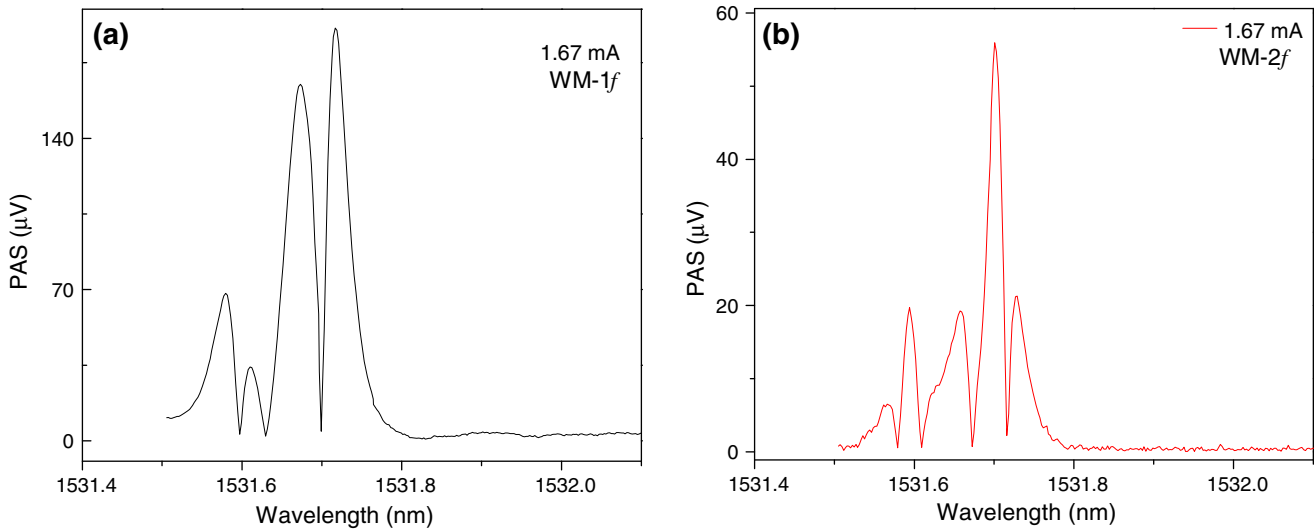
Fig. 6 Absolute PA spectrum in **a** WM-1*f* and **b** WM-2*f*. These measurements were taken in 1.67 mA modulation amplitude using 1,000 ppmv ammonia at 200 sccm flow rate

Fig. 7 PA spectrum broadening caused by the contribution of AM in WM-2*f*. The PA signal was normalized by the maximum value. These measurements were taken by increasing the modulation amplitude, but using the same high value of 350 mA of the injection current
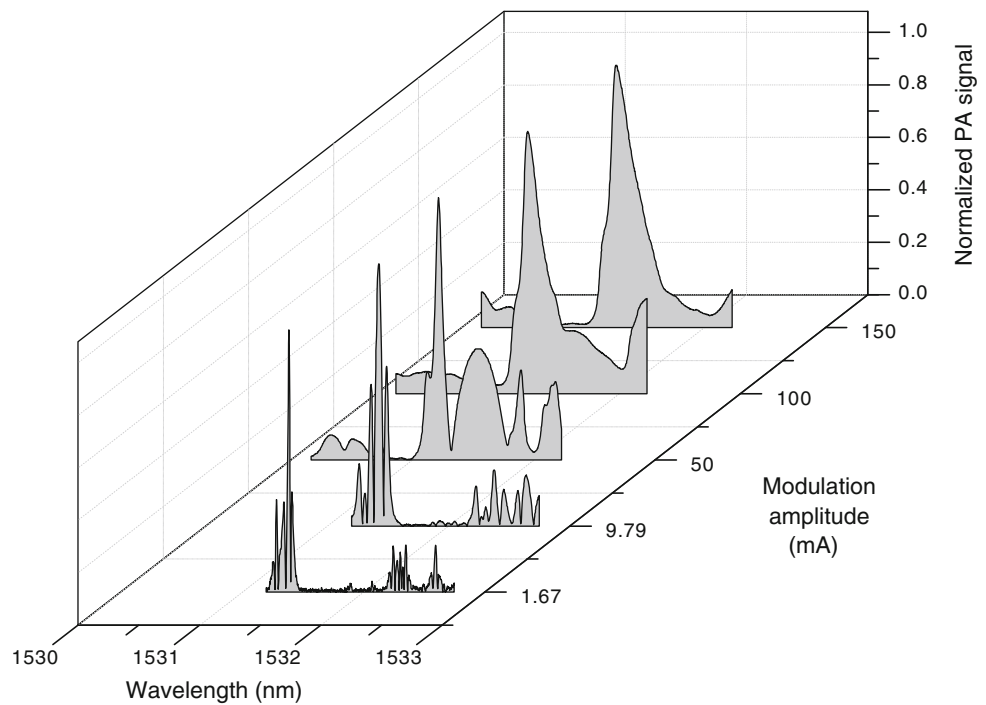
PA signal, U_{PA}, measured by the lock-in amplifier, can be regarded as a vectorial sum [8]:

$$U_{PA} = \left[S^2 + 2S\,Bg\cos(\theta_{PA} - \theta_{Bg}) + Bg^2 + N^2 \right]^{1/2} \quad (3)$$

where S is the true PA signal, i.e., generated only by the sample, Bg is the background, and N is the incoherent noise (microphone and flow noise). Considering the linear dependence of the PA signal on sample concentration c, by using a as the angular coefficient, the following function for the measured data can be applied:

$$U_{PA} = \left[(ac)^2 + bc + d^2 \right]^{1/2} \quad (4)$$

where the fitting parameter a is the sensitivity of the ammonia detector. By comparison of (3) and (4), the other fitting parameters can be obtained as follows: $b = 2a\,Bg\cos(\theta_{PA} - \theta_{Bg})$ and $d^2 = (Bg^2 + N^2)$.

Figure 8b shows the PA signal as function of the NH_3 concentration. Linear and nonlinear (Eq. 4) fits were accomplished. According to a linear fit (indicated by a dot-

Fig. 8 PA signal as a function of ammonia concentration starting from 12 to 124 ppbv fitted by Eq. (4). The *inset graph* shows a zoom of the sub-ppmv range fitted by Eq. (4) and a linear fit. For both fits, all data points were used. The *vertical error bars* correspond to the standard deviation of the PA signal over 500 points recorded at a rate of 1 point per second using the LabVIEW software. The *horizontal error bar* is associated with the accuracy of the mass flow controllers (± 0.5 % reading plus ± 0.1 % full scale). The *solid line* and *dot-dashed line* correspond to Eq. (4) and linear fit, respectively
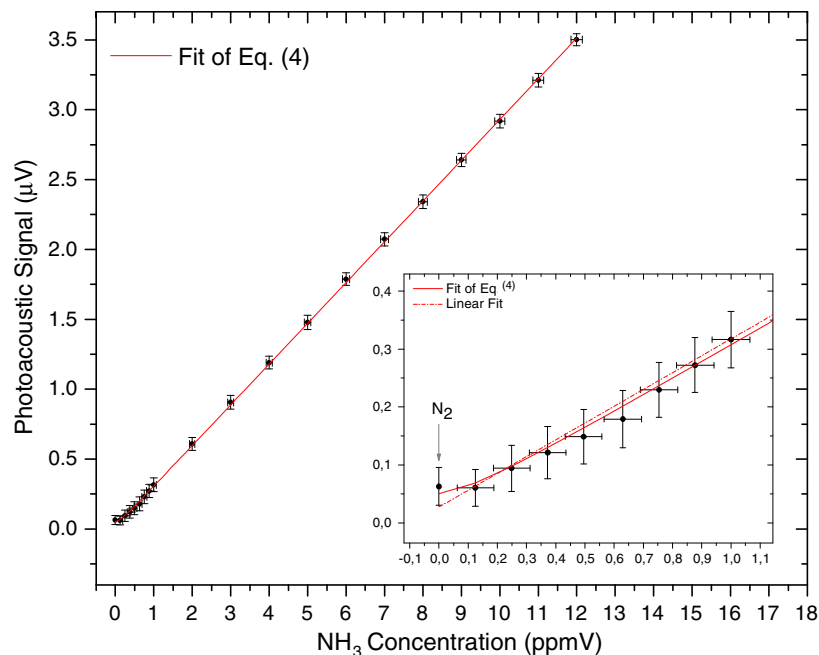
dashed line in the figure), a coefficient of determination $r^2 = 0.99981$ was found; meanwhile, by the means of Eq. (4), the obtained value for this coefficient was 0.99988. Choosing the Eq. (4) to determine the detection sensitivity and incoherent noise plus background of the PA sensor $(N + Bg)$, the estimated fitting parameters were $a = 0.29175 \pm 0.00091$ µV/ppmv, $b = 0.00689 \pm 0.00356$ (µV)^2/ppmv and $d = 0.05082 \pm 0.00807$ µV.

The standard deviation of the detection sensitivity, a, is smaller than 0.32 %. The parameter d gives the sum of incoherent noise and background. Therefore, the value of d should be close to the measured background in N_2 that is, as shown in Fig. 8, equals to 0.063 ± 0.032 µV, which is in good agreement considering the standard deviation. The ratio of d to a, 174 ppbv, expresses the $N + Bg$ in concentration. The average standard deviation (vertical error bars in Fig. 8) in the range from 0 to 1 ppmv is 0.043 µV. The ratio of this value to the detection sensitivity, 148 ppbv, can be regarded as the precision of the measurements expressed in concentration. Therefore, the limiting sensitivity is estimated as $174 + 2 \times 148 = 470$ ppbv at S/N = 1 and taken into account error bars. This is in agreement with the measured photoacoustic signal at 495 ppbv, which error bar do not overlap the corresponding error bar of the measured background signal.

In order to quantify the ammonia adsorption–desorption process, a study of the response time of the system was performed. Using the optimized configuration of the PA system, the rise time (10–90 %) in a concentration step from pure N_2 to 50 ppmv of ammonia in N_2 was

investigated at different flows. The results of these measurements can be seen in Figs. 9 and 10.

It can be seen in Fig. 9 that the curves approximate the same value of about 15 µV. Regarding this value as the true PA signal for 50 ppmv ammonia, the PA signals measured at different flow rates can be normalized by the true value. The normalized PA signals, expressed in percents, can be seen in Fig. 10. These curves can be used for determining the dependence of the accuracy of the photoacoustic concentration measurement in time. For achieving 10, 5 and 3 % deviation from the true concentration, the PA signal needs 12, 36 and 73 s time, respectively, at 200 sccm flow rate. At 50 sccm flow rate, 53, 122 and 185 s time would be needed for the same accuracy values. Depending on the application field, the PA ammonia sensor could be optimized for fast measurements with reduced accuracy, or for very accurate measurements with longer measurement time.

These results show clearly that the adsorption–desorption process, caused by the polar behavior of ammonia, increases the response time of the system. This effect can be minimized by increasing the flow rate. However, the use of higher flow rates may induce additional noise in the PA system which may limit the detection sensitivity. Another possibility for further reduction in the rise time would be the heating of the PA cell. A detailed study about adsorption–desorption process reports that its negative effects can be significantly reduced by heating the PA cell to 40–50 °C [26].

The cylindrical resonators of the PA cell are not coated by Teflon. Nevertheless, response times of 10–49 s for

Fig. 9 Comparison of the rise time using different flows. The *inset* shows an extended region of the graph
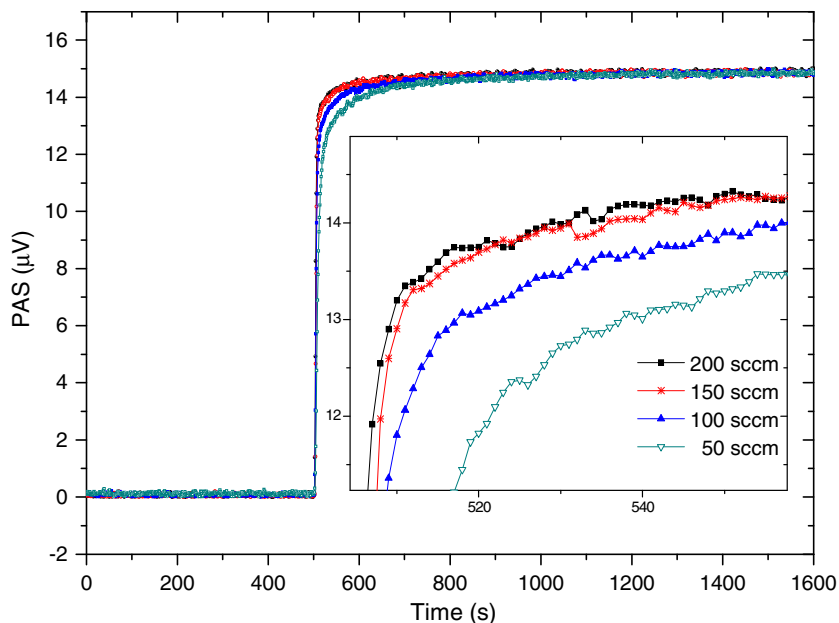
Fig. 10 Rise time values at different flows by considering the interval of 10–90 %. The *inset graph* is the calculated rise time as a function of the flux
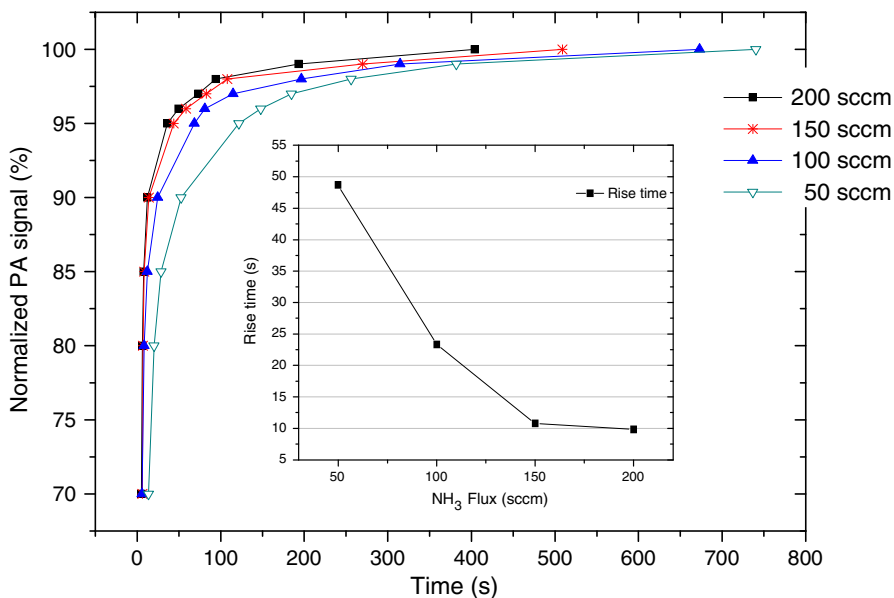
200–50 sccm flow rates have been found. These response time values enable the PA system to detect ammonia concentrations at ppbv level in applications that require real-time measurements.

5 Conclusion

A compact PA sensor using fiber-coupled DFB diode laser was developed to detect trace of ammonia at ppbv levels. The performance of the PA system was tested at several modulation configurations in order to optimize the detection sensitivity. The WM-2f with 8.2 mA of modulation amplitude proved to be the best modulation scheme to detect ammonia when compared with AM and WM-1f. A detection limit of 470 ppbv could be achieved. The results of ammonia adsorption–desorption measurements proved that the PA system can be utilized to detect low concentrations of ammonia in real time with high accuracy. The system features as the compact size of the PA cell and of the DFB laser combined with the possibility to replace the lock-in amplifier and the laser driver by digital signal processor (DSP)-based special electronic circuit are essential to build a portable, low cost and highly sensitive photoacoustic ammonia sensor.

References

1. S. MacDonald, N. Clecak, R. Wendt, C.G. Willson, C. Snyder, C. Knors, N. Deyoe, J. Maltabes, J. Morrow, A. McGuire, S. Holmes, Proc. SPIE **1466**, 2 (1991)
2. K. Pilegaard, J.K. Schjoerring, M.A. Sutton, Biogeoscience **6**, 3149–3150 (2009)
3. L.R. Narasimhan, W. Gordon, C.K.M. Patel, PNAS **98**, 4617–4621 (2001)
4. M. Wolff, H. Harde, Infrared Phys. Technol. **41**, 283–286 (2000)
5. A. Petzold, R. Niessner, Appl. Phys. Lett. **66**(10), 1285–1287 (1995)
6. Z. Bózóki, A. Mohácsi, G. Szabó, Z. Bor, M. Erdélyi, W. Chen, F.K. Tittel, Appl. Spectosc. **56**(6), 715–719 (2002)
7. R.A. Rooth, A.J.L. Verhage, L.W. Wouters, Appl. Opt. **29**, 3643 (1990)
8. A. Schmohl, A. Miklós, P. Hess, Appl. Opt. **41**(9), 1815–1823 (2002)
9. W. Zhang, Z. Wu, Q. Yu, Chin. Opt. Lett. **5**(11), 677–679 (2007)
10. A. Miklós, S. Schäfer, P. Hess, in *Encyclopedia of Spectroscopy and Spectrometry*, ed. by J.C. Lindon, G.E. Tranter, J.L. Homes (Academic Press, San Diego, 2000), pp. 1815–1822
11. A. Miklós, P. Hess, Z. Bózóki, Rev. Sci. Instrum. **72**(4), 1937–1955 (2001)
12. F. Harren, R.J. Reuss, Asads sd, in *Encyclopedia of Applied Physics*, vol. 19, ed. by G.L. Trigg (VCH, Weinheim, 1997), pp. 413–435
13. P. Hess, Top. Curr. Chem. **111**, 1–32 (1983)
14. M.W. Sigrist, Rev. Sci. Instrum. **74**, 486–490 (2003)
15. M.W. Sigrist, *Air Monitoring by Spectroscopic Techniques* (Wiley-Interscience Publication, New York, 1994), p. 127
16. S. Sthéphane, L. Thévenaz, Spectrochim. Acta A **60**, 3259–3268 (2004)
17. J. Li, X. Gao, L. Fang, Opt. Laser Technol. **39**, 1144–1149 (2007)
18. J.S. Pilgrim, D.S. Bomse, Wavelength modulation photoacoustic spectrometer. United States Patent number 6,552,792 B1 (2003)
19. J. Wang, W. Zhang, L. Li, Appl. Phys. B **103**(2), 263–269 (2011)
20. S. Sthéphane, L. Thévenaz, Infrared Phys. Technol. **48**, 154–162 (2006)
21. R. Arndt, J. Appl. Phys. **36**, 2522–2524 (1965)
22. Y. Peng et al., Spectrochim. Acta A Mol. Biomol. Spectrosc. **74**, 924–927 (2009)
23. J. Reid, D. Labrie, Appl. Phys. B **26**, 203–210 (1981)
24. L.C. Philippe, R.K. Hanson, Appl. Opt. **32**, 6090–6103 (1993)
25. J.P. Benson, S. Schilt, L. Thévenaz, Proc. SPIE **5855**, 415–418 (2005)
26. A. Schmohl, A. Miklós, P. Hess, Appl. Opt. **40**, 2571–2578 (2001)
27. S.W. Sharpe, T.J. Jhonson, R.L. Sams, P.M. Chu, G.C. Rhoderick, P.A. Jhonson, Appl. Spectrosc. **58**, 1452–1461 (2004)